CONTRAST MEDIA & MOLECULAR IMAGING

Received: 25 June 2009, Revised: 1 February 2010, Accepted: 2 February 2010, Published online in Wiley InterScience: 7 May 2010

(www.interscience.wiley.com) DOI:10.1002/cmmi.374

Development of magnetic chromatography to sort polydisperse nanoparticles in ferrofluids

Delphine Forge[a], Yves Gossuin[b], Alain Roch[a], Sophie Laurent[a], Luce Vander Elst[a] and Robert N. Muller[a]*

Whatever the strategy of synthesis, nanoparticles in magnetic fluids commonly feature a broad size distribution. However, the presence of several size populations in ferrofluids is often problematic because of the close relationship between the efficiency of the nanoparticles and their physicochemical properties. In this work, a magnetic size sorting procedure is developed in order to reduce this polydispersity, using the magnetic properties of the iron oxide nanoparticles. This magnetic sorting with an adjustable magnetic field allows isolation of the small superparamagnetic particles as well as the larger particles. Magnetometry, nuclear magnetic relaxation dispersion profiles and transmission electron microscopy were successfully used to check the efficiency of the magnetic sorting procedure, which was shown to work as a 'magnetic' chromatography. Copyright © 2010 John Wiley & Sons, Ltd.

Keywords: magnetic fluid; magnetic chromatography; monodispersity; biomedical applications

1. INTRODUCTION

Applications of superparamagnetic iron oxide nanoparticle suspensions (ferrofluids) are in constant development in the biomedical field (1–3) including magnetic resonance imaging (MRI) (4,5), tissue repair, hyperthermia, drug delivery, cell separation and cell labeling. Each of these applications requires a specific type of nanoparticles (i.e. a high magnetization value, a peculiar surface coating or an appropriate size). The size distribution of the particles is a very important characteristic of these materials since it influences their efficiency for these different applications. For MRI contrast agents, two kinds of particles can be considered (6): (i) large particles (hydrodynamic diameter $d_H > 30$ nm), called superparamagnetic iron oxide particles (SPIOs), used for liver imaging; and (ii) smaller particles ($d_H < 30$ nm), called ultrasmall SPIOs (USPIOs), used for MR angiography. The differences between SPIO and USPIO are the longer blood half-life and the lower transversal relaxivity, r_2, of the latter (Table 1). Indeed, the hydrodynamic diameter of the particles is an important factor determining the pharmacokinetics and biodistribution of a contrast agent. The characteristics of USPIOs open up new clinical applications such as the targeting of organs other than those belonging to the reticuloendothelial system (RES). Moreover, a broad size distribution can also be responsible for the instability of the colloidal suspension. It is a real challenge to provide efficient and specific monodisperse magnetic fluids (containing a single size distribution), in particular for biomedical applications.

There are many procedures allowing the synthesis of magnetic nanoparticles. According to the experimental procedure, the size, shape and monodispersity can be controlled (7–12). For example, the reactions in constraint environments or the thermal decomposition of iron organic precursors such as $Fe(CO)_5$ or $Fe(acac)_3$ using organic solvents and surfactants allows the direct formation of nanocrystals characterized by a high monodispersity without any method of separation.

Unfortunately, the coprecipitation method, which is the simplest and most efficient chemical pathway to obtain magnetite, generally produces polydisperse iron oxide nanoparticles (presenting more than one size population). This polydispersity is often characterized by a lognormal probability distribution (13):

$$P(r) = \frac{1}{\sigma r\sqrt{2\pi}} \exp\left[-\frac{\ln^2(r/r_0)}{2\sigma^2}\right] \quad (1)$$

with r_0 being the median radius value and σ the standard deviation.

Many studies (14,15) have explained this polydispersity by the Brownian coagulation model. Another model (16), based on a random residence time approach, proposes that particles are moving by diffusion and drift through a finite growth zone. The particle size is assumed to be a power function of growth time, and the final size distribution is determined by the first passage time.

* *Correspondence to: R. N. Muller, Department of General, Organic and Biomedical Chemistry, NMR and Molecular Imaging Laboratory, University of Mons, B-7000 Mons, Belgium.*
E-mail: robert.muller@umons.ac.be

a *D. Forge, A. Roch, S. Laurent, Luce Vander Elst, R. N. Muller*
Department of General, Organic and Biomedical Chemistry, NMR and Molecular Imaging Laboratory, University of Mons, 24 Avenue du Champ de Mars, B-7000 Mons, Belgium

b *Y. Gossuin*
Biological Physics Department, University of Mons, 24 Avenue du Champ de Mars, B-7000 Mons, Belgium

Contract/grant sponsors: COST Action D38, EMIL NoE Program, NOMADE Program of the Walloon Region.
Contract/grant sponsor: ENCITE (7th FP); contract/grant number: 201841.
Contract/grant sponsor: ARC Program of the French Community of Belgium.

Table 1. Physicochemical characteristics of typical USPIO (AMI-227) and SPIO (AMI-25)

	Hydrodynamic size (nm)	r_1 (1/s mM) 20 MHz	r_2 (1/s mM) 20 MHz	r_2/r_1 20 MHz	Applications
AMI-227	28	24	53	2.2	Blood pool imaging, cellular labeling, lymph nodes imaging
AMI-25	80–150 polydisperse	24	98	4.1	Liver imaging, cellular labeling

Several methods for the separation of the particle populations according to size have been proposed during recent years. These techniques (17–20) are often based on physical processes such as ultracentrifugation, microfiltration, or the well-known size exclusion chromatography (SEC) (21). One disadvantage of SEC is the need to add electrolytes, which often destabilizes the magnetic fluid and its removal. Furthermore, very large particles can clog the column. However, size sorting selection may also be performed by adding an electrolyte solution or a nonsolvent to the colloidal solution to disrupt its stability (22). This causes larger particles to precipitate and leaves smaller particles in the supernatant as a nearly monodisperse population.

Another size-selective technique is the flow field-flow fractionation (FFFF) (23). In this case, the separation is carried out in a flow with a parabolic profile running through a thin channel. A field (gravitational, centrifugal, magnetic, thermal or a cross flow of fluids) is applied along an axis perpendicular to the flow axis in order to cause separation due to the different mobility of the various components in the field. FFFF does not require electrolyte solutions and expensive separation materials and is not restricted to smaller particle sizes. However, up to now, FFFF has not been available as a preparative method: it is only used for the analytical fractionation of magnetic fluids.

In this work, we propose a size-selection method exploiting the magnetic properties of the crystals. The main advantages of this method are its speed, its low cost and its easy implementation. Another advantage of magnetic sorting is certainly its capacity to accommodate the physicochemical properties of the ferrofluid (i.e. USPIO or SPIO) according to the final application considered.

As previously described (24,25), the analysis of the nuclear magnetic relaxation dispersion (NMRD) profiles and of the magnetometric curves, completed by the transmission electron microscopy (TEM) images, can be used to characterize the different fractions. This procedure will be exploited to assess the efficiency of the new size separation process, which is closer to a 'magnetic chromatography' than to a simple filtration.

2. MATERIALS AND METHODS

2.1. Instruments

The magnetic fractions were characterized by various techniques. The magnetization measurements were performed on a known amount of ferrofluid using a vibrating sample magnetometer (VSM-Nuovo Molspin, Newcastle-upon-Tyne, UK). The error on a magnetization measurement was about 4%. The fitting of the Langevin function [eqn (2)] to the magnetometric profiles provides important information such as the crystal radius (r) and the specific magnetization (M_{sat}) (26):

$$M = M_{sat} L(x) \tag{2}$$

where $L(x) = \coth(x) - (1/x)$ is the Langevin function and $x = \mu B_0 / k_B T$ with μ the magnetic moment of the particle, k_B the Boltzmann constant and T the absolute temperature.

An additional way of determining the size is the measurement of the proton nuclear magnetic relaxation rate of water at different magnetic fields. Nuclear magnetic relaxation dispersion profiles were recorded with a fast field cycling relaxometer (Stelar, Mede, Italy) measuring the longitudinal relaxation rates (R_1) over a field range extending from 0.24 mT to 0.24 T. The temperature of the samples was adjusted to 37 °C with a precision of 0.1 °C. Additional longitudinal (R_1) and transverse (R_2) relaxation rate measurements at 0.47 and 1.41 T were obtained on Minispec PC 120 and Mq 60 spin analyzers (Bruker, Karlsruhe, Germany). The fitting of the NMRD profiles by a theoretical relaxation model (27,28) [eqn (3)] allows the determination of the crystal radius (r), the specific magnetization (M_{Sat}) and the Néel relaxation time (τ_N).

$$R_1 = \frac{32\pi}{135000}\mu^2\gamma^2\frac{N_a C}{rD}\left[\begin{array}{l} 7P\frac{L(x)}{x}J_F(\omega_s,\tau_D,\tau_N)+ \\ \left[7(1-P)\frac{L(x)}{x}+3(1-2\frac{L(x)}{x}+L^2(x))\right]J_F(\omega_I,\tau_D,\tau_N)+3L^2(x)J_A(\omega_I,\tau_D)\end{array}\right] \tag{3}$$

where, in cgs units, ω_I is the proton larmor angular frequency, ω_S is the electron larmor angular frequency, $\tau_D = r^2/D$ is the translation correlation time of the particle, D is the water diffusion coefficient, γ is the proton gyromagnetic ratio, C is the particle concentration, N_a is the Avogadro number and μ is the magnetic moment of the particle. The model is only valid for small and unclustered particles. Therefore, the results of the fitting are not provided in Table 2 when the particles are too large or clustered.

The fits of magnetization curves and NMRD profiles are obtained using a single monodisperse radius for nanoparticles. The size and the shape of the particles were determined using transmission electron microscopy (MET; CM 20, Philips, USA). A small volume of the sample was vaporized on carbon-coated copper grids in order to avoid artificial aggregation of the particles upon sample drying. Hydrodynamic sizes (d_H) were measured on a Zêtasizer Nanoseries ZEN 3600 (Malvern, UK).

Table 2. Physicochemical characteristics of initial sample and of fractions 1 and 2 obtained according to the magnetic field of sorting

	r_1 (1/s mM) 20 MHz	r_2 (1/s mM) 20 MHz	r_2/r_1 20 MHz	r_2/r_1 60 MHz	Hydrodynamic size (nm)	r_{relaxo} (nm)	$r_{magneto}$ (nm)	PI
Amino ferrofluid	49.5	145.5	2.98	6.8	29 polydisperse	5.9	5.2	0.13
2000 G Fraction 1	31.8	54.7	1.72	3	16 monodisperse	4.4	4.2	0.05
2000 G Fraction 2	43.9	140.6	3.2	6.4	25 monodisperse	5.2	4.9	0.06
1000 G Fraction 1	46.4	95.2	2.05	3.91	17 monodisperse	5.03	4.8	0.05
1000 G Fraction 2	32.7	207.9	6.35	8.26	27 monodisperse	6.4	6	0.066
750 G Fraction 1	46.3	99.5	2.15	4.33	18 monodisperse	5.3	5	0.06
750 G Fraction 2	36.1	249.4	6.9	11.96	42 monodisperse	7	6	0.15
500 G Fraction 1	48.5	109.6	2.26	4.69	24 polydisperse	5.5	5	0.1
250 G Fraction 1	49.1	132.6	2.7	6.81	28 polydisperse	5.8	5.2	0.11

The total iron concentration was determined by the measurement of the longitudinal relaxation rate R_1 according to the method previously described (29). Briefly, the samples were mineralized by microwave digestion (MLS-1200 Mega, Milestone, Analis, Namur, Belgium) and the R_1 value of the resulting solutions was recorded at 0.47 T and 37 °C which allowed determining iron concentration, using eqn (4):

$$[\mathrm{Fe}] = (R_1{}^{\mathrm{sample}} - R_1{}^{\mathrm{diam}}) * 0.0915 \qquad (4)$$

where R_1^{diam} (s^{-1}) is the diamagnetic relaxation rate of acidified water (0.36 s^{-1}) and 0.0915 (s mM) is the slope of the calibration curve.

2.2. Chemicals and magnetic size sorting

The magnetic fluids used for these experiments were generated in a two-step process. The γ-Fe_2O_3 nanoparticles were first prepared by a co-precipitation method described previously (30). The iron oxide particles were then coated with γ-aminopropyltrimethoxysilane (31).

The magnetic sorting was carried with magnetic separation columns (Miltenyi Biotec BU, Utrecht, The Netherlands, LS column MACS). Figure 1 shows the scheme of the experimental apparatus.

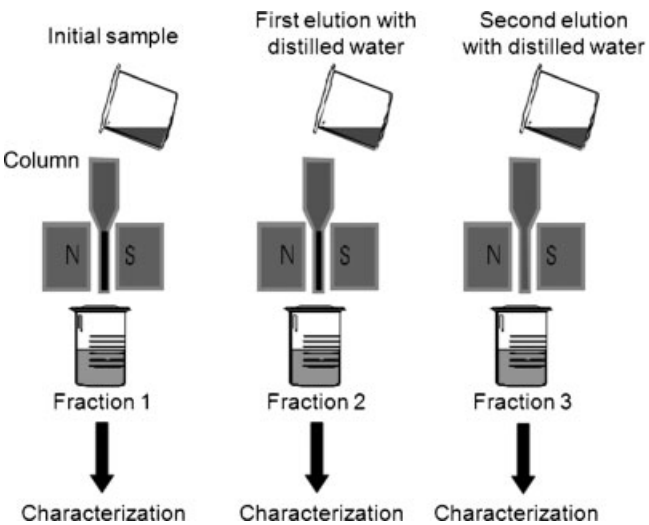

Figure 1. Strategy of magnetic chromatography.

When placed in an electromagnet, the MACS column matrix creates strong magnetic field gradients retaining magnetic particles according to their global magnetic moments and hence to their sizes. The mechanism of particle capture in the gradients has been identified from force and momentum balance equations (magnetic and hydrodynamic) in the capture areas (32).

For each size sorting, 5 ml of 50 mM aminoferrofluid (corresponding to about 10^{15} particles) was put into the column. The separation is essentially gravitational; there is no elution flow control. In this work, we characterized the particles which were not retained in the column. The magnetic fields used for the first separation ranged from 250 to 2000 G.

For a successive size sorting experiment, each elution was performed with 3 ml of distilled water. This experimental procedure made it possible to realize up to three successive sizes sorting under the same magnetic field (750, 1000 and 2000 G).

3. RESULTS AND DISCUSSION

3.1. Evaluation of the size sorting procedure

Numerous methods can be used to determine the size of magnetic nanoparticles. However, the polydispersity of the colloidal solution leads to different mean values (even if characterizing the same sample) since the different techniques are sensitive to a number (r), a volume (r^3), or even an intensity (r^6) (33). In the last two cases, the mean size is distorted toward high values because of the presence of small quantities of very large nanoparticles.

TEM analysis certainly represents the best technique for the determination of particle size (since the mean is weighted in number) as well as for the evaluation of the size distribution and the shape. This technique requires an image analysis based on a statistically significant number of particles. It is not realistic to analyze each sample with this time- and money- consuming technique.

Therefore, the strategy developed in this work consisted first in comparing the radius obtained by magnetometry and relaxometry. The radius obtained by magnetometry is a volume-weighted mean value, whereas the one obtained by relaxometry is an intensity-weighted mean value. The differ-

ence between those values can be a good parameter to assess the broadness of the particle size distribution. Equality between the radius values would reflect a very narrow size distribution, while a broad size distribution would result in a large difference between the values obtained by magnetometry and relaxometry.

Based on those measurements, the polydispersity index (PI) has been defined to evaluate the size distribution:

$$PI = \frac{r_{relaxo} - r_{magneto}}{r_{magneto}} \quad (5)$$

The smaller the PI, the narrower is the size distribution. Throughout this study, TEM measurements were also performed in order to validate the results. It should be noted that an alternative method (34), based only on magnetometric curves, allows the parameters of the size distribution to be obtained. However, we preferred to use the approach described above, since our magnetometric measurements present a quite large uncertainty (4%).

3.2. Magnetic chromatography of polydisperse ferrofluids

Standard magnetic amino fluids are often polydisperse. They were therefore filtered magnetically at fields between 250 and 2000 G. The relaxometric properties, the crystal radius and the hydrodynamic size of the initial sample and of the different fractions are shown in Table 2. As can be seen, magnetic sorting significantly modifies the physicochemical properties of iron oxide crystals. Figure 2(a) compares the NMRD profiles of the original suspension and of the different fractions, while Fig. 2(b) present the corresponding magnetometric curves. The difference between these profiles reflects an evolution of the particle size distribution during magnetic sorting. At a field of 2000 G, the obtained magnetic fluid is monodisperse, with a small PI. However, the relaxivity of this fraction is too weak for it to be used as an MRI contrast agent. Moreover, this fraction is characterized by a very low iron concentration (about 7 mM). On the contrary, the colloidal dispersion filtered at 250 G is characterized by larger particles and an interesting relaxivity but the polydispersity is similar to the initial sample (high PI and three populations). According to these results, a field ranging between 750 and 1000 G is optimal to obtain an appropriate magnetic fluid. Indeed, the small particles obtained in these conditions are characterized by interesting relaxivities, a high saturation magnetization, a weak polydispersity index, a small r_2/r_1 ratio, and a hydrodynamic diameter typical of an USPIO.

In order to assess accurately the size distribution of these fractions, an analysis of TEM images was performed (Fig. 3). The size histograms show the efficiency of the separation method, particularly by eliminating the larger particles. At a field of 750 G, the intensity of the magnet is less efficient in the retention of larger particles. Magnetic sorting also modifies the shape of the distribution, as shown by the fact that only at 2000 G the distribution of the fractions filtered is typically Gaussian whereas at the other magnetic fields it is not. To facilitate the comparison in this work, the data resulting from all size histograms are calculated assuming a log–normal distribution (Table 3).

The only quantitative argument that can be used for judging the narrower size distribution is the standard deviation σ between the different fractions. A decrease of the mean radius and of the standard deviation σ is observed for larger sorting magnetic fields. The difference between the values can seem negligible, but it is very significant since these standard deviations were obtained by the log–normal adjustment of the distribution. It is thus the standard deviation of the Gaussian distribution of the logarithms of the radius values.

The optimal field seems to be around 1000 G. It is however impossible to specify a universal sorting magnetic field, since it will obviously depend on the physicochemical characteristics of the initial sample. These results also allow validating our screening method to evaluate the sample polydispersity. This method will be used preferentially in the rest of this study, because of its rapidity.

The colloidal solution obtained at 1000 G remains stable at physiological pH during more than 2 weeks, as shown by the nearly constant value of r_2/r_1 at 1.41 T. Indeed, agglomeration causes an increase in the transverse relaxation rate and an attenuation of the longitudinal relaxation (35); therefore the ratio r_2/r_1 is a good indicator of the aggregation level of superparamagnetic colloids.

For biomedical applications, it is also interesting to obtain large and monodisperse particles, which are characterized by a higher relaxivity than USPIOs. For this purpose, a second separation process was developed to collect those particles of larger radius

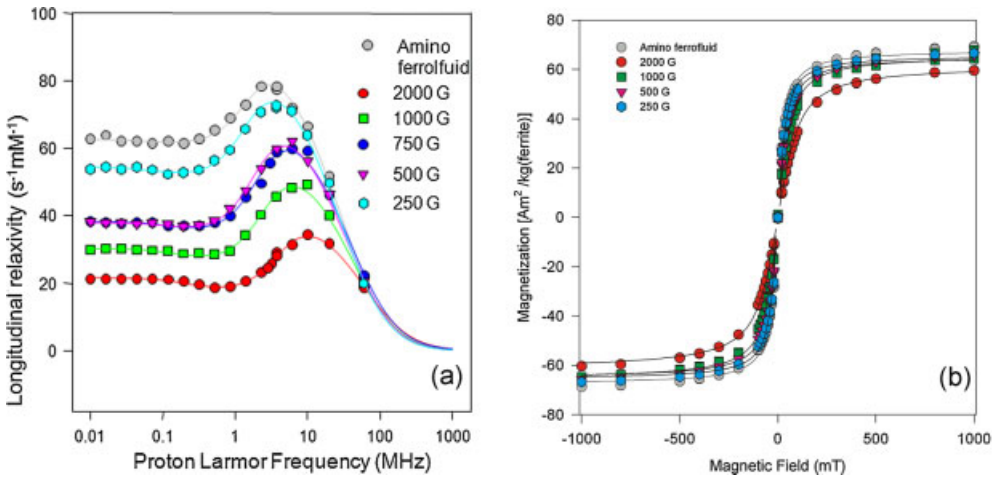

Figure 2. NMRD profiles (a) and magnetometric curves (b) of amino ferrofluid and of the fractions obtained after sorting at different magnetic fields. Lines are theoretical fits to the data.

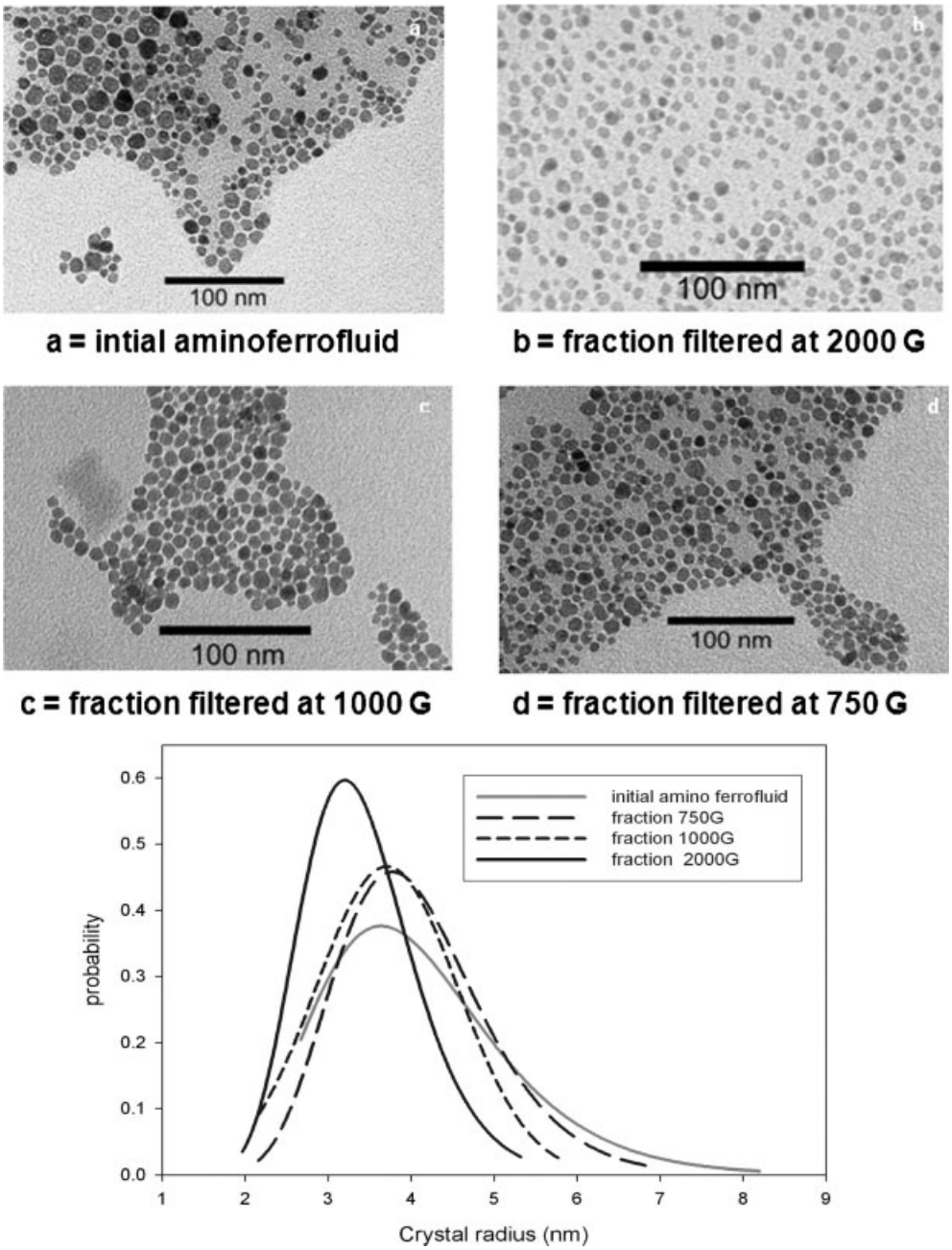

Figure 3. TEM images of the amino ferrofluid and the fractions obtained after sorting at different fields and comparison of the particle size distributions (lognormal adjustment).

Table 3. Median radius and standard deviation of initial sample and of fraction 1 (2000, 1000 and 750 G) obtained from a log–normal adjustment of size histograms

	Median radius (nm)	Standard deviation σ
Amino ferrofluid	3.9	0.28
2000 G Fraction 1	3.3	0.2
1000 G Fraction 1	3.8	0.23
750 G Fraction 1	4	0.22

that were retained in the column during the first filtration. After this latter, a second fraction (fraction 2) was obtained thanks to the elution with distilled water, still under the magnetic field. The physicochemical characteristics of the initial amino ferrofluid as well as of each fraction for different magnetic fields (2000, 1000 and 750 G) are also included in Table 2. For all magnetic fields, the hydrodynamic size measurement of fractions 1 and 2 still shows the presence of only one population. All the samples corresponding to the second fraction present a higher transversal relaxivity than the first fraction samples and the initial sample. Indeed these nanoparticles are characterized by a more important radius. The r_2/r_1 ratio and the mean hydrodynamic diameter are definitely higher for the second fraction. This

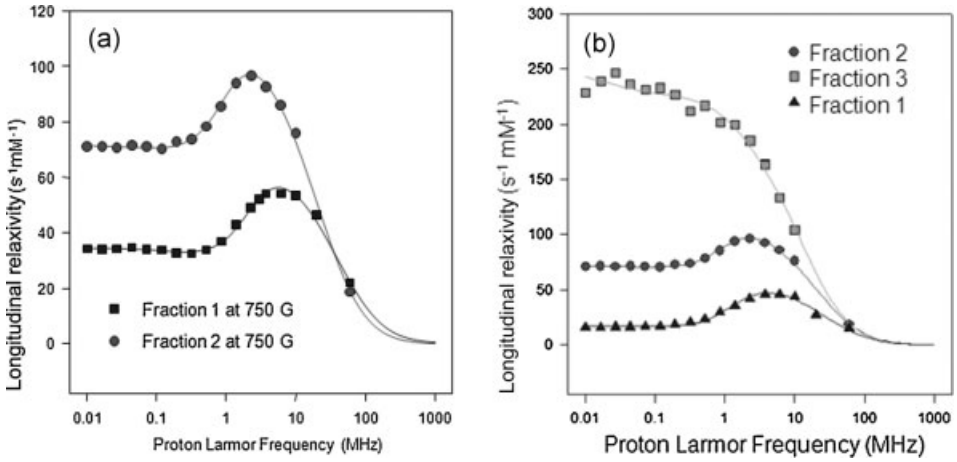

Figure 4. NMRD curves of (a) fractions 1 and 2 (before and after one elution with water) obtained at a field of 750 G and of (b) fractions 1, 2, and 3 obtained with a magnetic field of 1000 G. Lines are theoretical fits to the data.

fraction is thus constituted by the larger particles present in the lognormal size distribution of the initial sample. Figure 4(a) clearly shows an increase in the relaxivity after water elution (at a 750 G field). The properties of these 'eluted' particles depend on the magnetic field and on the number of elutions. For a high magnetic field, the quantity of collected particles is very weak for fraction 1 since they are more efficiently retained in the magnetic field. Consequently, the quantity of particles recovered during the second sorting is more important. A second elution, i.e. the third magnetic sorting (fraction 3), is only possible for relatively strong fields (2000 and 1000 G). A sorting field of 750 G seems insufficient to allow an effective separation of the various populations of particles present in the sample. For weak magnetic fields, the dynamics of sorting is indeed faster, causing a less effective separation of the magnetic grains. A field value of 1000 G seems to be a good compromise to obtain ferrofluids characterized by interesting relaxometric properties.

Our magnetic sorting thus allows modulation of the crystal radius according to the sorting field and the number of elutions. This modulation is confirmed by the analysis of the shape of NMRD profiles. Figure 4(b) shows the NMRD profiles of the different fractions for a 1000 G sorting field. The profile of fraction 1 presents an inflection point at a relatively high field, which confirms the presence of small particles; whereas for fraction 3, the relaxivity maximum at intermediate field has completely disappeared, suggesting the existence of larger and/or clustered particles ($r_{magneto} = 6.8$ nm and $d_H = 98$ nm). The NMRD profiles are thus very sensitive to the size distribution of the magnetic crystals.

Magnetic filtration is often used for a unique separation. Our results prove that multiple fractions can be obtained from a single sample during the same experiment, simply by using successive elutions. However, it is not clear why additional elutions are capable of detaching particles from the column. The gradients are clearly modifying the flow properties of the initial ferrofluid, since we observed a significant increase in the flow time of the first sorting for increasing magnetic fields (and thus increasing gradients). Therefore, when performing the first elution with non-magnetic distilled water, the physical parameters of the interaction between the particles and the column are modified. This seems to allow the detachment of particles captured in the column during the initial sorting.

Contrary to all appearances, this size sorting process can thus be seen (and used) as a dynamic phenomenon, such as a chromatographic technique.

4. Conclusions

A new separation method that clearly allows a refinement of the size distribution based on magnetic field gradients was developed. In this process, the magnetic properties of the particles are exploited in an advantageous way. The size of the magnetic grains and consequently the relaxometric properties of the ferrofluid can be changed by choosing the appropriate magnetic field and the number of water elutions. According to the experimental conditions, it is possible either to isolate particles with characteristics close to USPIOs, or to collect SPIO particles. These first results are very encouraging and could open many industrial prospects. This 'magnetic chromatography' could significantly help to optimize magnetic fluids for different applications.

Acknowledgements

The authors thank Materia Nova for the TEM studies. D.F. is grateful to the FRIA for financial support. Sponsorship from the COST Action D38, EMIL NoE Program, NOMADE Program of the Walloon Region, ENCITE (7th FP, grant no. 201841) and the ARC Program of the French Community of Belgium is kindly acknowledged.

REFERENCES

1. Laurent S, Forge D, Port M, Roch A, Robic C, Vander Elst L, Muller RN., Magnetic iron oxide nanoparticles: synthesis, stabilization, vectorization, physicochemical characterizations, and biological applications. Chem Rev 2008; 108: 2064–2110.
2. Gupta AK, Gupta M. Synthesis and surface engineering of iron oxide nanoparticles for biomedical applications. Biomaterials 2005; 26: 3995–4021.
3. Rosensweig RE. Heating magnetic fluid with alternating magnetic field. J Magn Magn Mater 2002; 252: 370–374.
4. Boutry S, Laurent S, Vander Elst L, Muller RN., Specific E-selectin targeting with a superparamagnetic MRI contrast agent. Contrast Med Mol Imag 2006; 1: 15–22; doi: 10.1002/cmmi.87
5. Lawaczeck R, Menzel M, Pietsch H. Superparamagnetic iron oxide particles: contrast media for magnetic resonance imaging. Appl Organometal Chem 2004; 18: 506–513; doi: 10.1002/aoc.753
6. Jung CW, Jacobs P. Physical and chemical properties of superparamagnetic iron oxide MR contrast agent: ferumoxides, ferumoxtran, ferumoxsil. Magn Reson Imag 1995; 13: 661–674.

7. Corti M, Lascialfari A, Micotti E, Castellano A, Donativi M, Quarta A, Cozzoli PD, Manna L, Pellegrino T, Sangregorio C. Magnetic properties of novel superparamagnetic MRI contrast agents based on colloidal nanocrystals. J Magn Magn Mater 2008; 320: e320–e323.
8. Song H-T, Choi J-S, Huh Y-M, Kim S, Jun Y-W, Suh J-S, Cheon J. Surface modulation of magnetic nanocrystals in the development of highly efficient magnetic resonance probes for intracellular labeling. J Am Chem Soc 2005; 127: 9992–9993.
9. Jun Y-W, Huh Y-M, Choi J-S, Lee J-H, Song H-T, Kim S, Yoon S, Kim K-S, Shin J-S, Suh J-S, Cheon J. Nanoscale size effect of magnetic nanocrystals and their utilization for cancer diagnosis via magnetic resonance imaging. J Am Chem Soc 2005; 127: 5732–5733.
10. Cozzoli PD, Snoeck E, Garcia M, Giannini C, Guagliardi A, Cervellino A, Gozzo F, Hernando A, Achterhold K, Ciobanu N, Parak F, Cingolani R, Manna L. Colloidal synthesis and characterization of tetrapod-shaped magnetic nanocrystals. Nano Lett 2006; 6: 1966–1972 .
11. Boni A, Marinone M, Innocenti C, Sangregorio C, Corti M, Lascialfari A, Mariani M, Orsini F, Poletti G, Casula MF. Magnetic and relaxometric properties of Mn ferrites. J Phys D Appl Phys 2008; 41: 134021–134027.
12. Lartigue L, Oumzil K, Guari Y, Larionova J, Guérin C, Montero J-L, Barranga-Montero V, Sangregorio C, Caneschi A, Innocenti C, Kalaivani T, Arosio P, Lascialfari A. Water-soluble rhamnose-coated Fe_3O_4 nanoparticles. Org Lett 2009; 11: 2992–2995.
13. Blanco-Mantecon M, O'Grady K. Grain size and blocking distributions in fine particle iron oxide nanoparticles. J. Magn. Magn. Mater. 1999; 203: 50–53.
14. Lee KW, Lee YJ, Han DS. The log–normal size distribution theory for Brownian coagulation in the low Knudsen number regime. J Colloid Interface Sci 1997; 188: 486–492.
15. Kim DS, Hong SB, Kim YJ, Lee KW. Deposition annd coagulation of polydisperse nanoparticles by Brownian motion and turbulence. Aerosol Sci 2006; 37: 1781–1787.
16. Kiss LB, Soderlünd J, Niklasson GA, Granqvist CG. The real origin of lognormal size distributions of nanoparticles in vapor growth processes. Nanostruct Mater 1999; 12: 327–332.
17. Peralez-Perez O, Sasaki H, Kasuya A, Jeyadevan B, Tohji K, Hihara T, Sumiyama K. Production of monodispersed particles by using effective size selection. J Appl Phys 2002; 91: 6958–6960.
18. Mefford OT, Carroll MRJ, Vadala ML, Goff JD, Mejia-Ariza R, Saunders M, Woodward RC, St Pierre TG, Davis RM, Riffle JS. Size analysis of PDMS-magnetite nanoparticle complexes: experiment and theory. Chem Mater 2008; 20: 2184–2191.
19. Ngomski AF, Bee A, Draye M, Cote G, Cabuil V. Magnetic nano- and microparticles for metal removal and environmental applications: a review. C R Chim 2005; 8: 963–970.
20. De Cuyper M. Applications of magnetoproteoliposomes in bioreactors operating in high-gradient magnetic fields. In Handbook of Nonmedical Applications of Liposomes – From Design to Microreactors, Barenholz Y, Lasic DD (eds). CRC Press: Boca Raton, FL, 1995; 325–342.
21. Hur J, Schlautman MA. Effects of pH and phosphate on the adsorptive fractionation of purified Aldrich humic acid on kaolitine and hematite. J Colloid Interface Sci 2004; 277: 264–270.
22. Massart R, Dubois E, Cabuil V, Hasmonay E. Preparation and properties of monodisperse magnetic fluids. J Magn Magn Mater 1995; 149: 1–5.
23. Rheinländer T, Roessner D, Weitschies W, Semmler W. Comparison of size-selective techniques for the fractionation of magnetic fluids. J Magn Magn Mater 2000; 214: 269–275.
24. Ouakssim A, Roch A, Pierart C, Muller RN. Characterization of polydisperse superparamagnetic particles by nuclear magnetic relaxation dispersion (NMRD) profiles. J Magn Magn Mater 2002; 252: 49–52.
25. Ouakssim A, Fastrez S, Roch A, Laurent S, Gossuin Y, Pierart C, Vander Elst L, Muller RN., Control of the synthesis of magnetic fluids by relaxometry and magnetometry. J Magn Magn Mater 2004; 272: e1711–e1713.
26. Rosensweig RE. Ferrohydrodynamics. Cambridge University Press: Cambridge, 1985.
27. Muller RN, Vander Elst L, Roch A, Peters JA, Csajbok E, Gillis P, Gossuin Y., Relaxation by metal-containing nanosystems. Adv Inorg Chem 2005; 57: 239–292; doi: 10.1016/S0898-8838(05)57005-3
28. Roch A, Muller RN, Gillis P. Theory of proton relaxation induced by superparamagnetic particles. J Chem Phys 1999; 110: 5403–5411.
29. Boutry S, Forge D, Burtea C, Mahieu I, Murariu O, Laurent S, Vander Elst L, Muller R.N., How to quantify iron in an aqueous or biological matrix: a technical note. Contrast Media Mol Imag 2009; 4: 1–6.
30. Forge D, Roch A, Laurent S, Tellez H, Gossuin Y, Renaux F, Vander Elst L, Muller RN., Optimization of the synthesis of superparamagnetic contrast agents by the design of experiments method. J Phys Chem 2008; 112: 19178–19185; doi: 10.1021/jp803832k
31. Mornet S, Portier J, Duguet E. A method for synthesis and functionalization of ultrasmall superparamagnetic covalent carriers based on maghemite and dextran. J Magn Magn Mater 2005; 293: 127–134; doi: 10.1016/j.jmmm.2005.01.053
32. Abbasov T. Magnetic filtration with magnetized granular beds: basic principles and filter performance. China Particuol 2007; 5: 71–83.
33. Roch A, Lucet I, Pouliquen D, Anseau M, Muller RN. Proceedings of the International Society for Magnetic Resonance in Medicine, New York, 1996; 70.
34. Andhariya N, Chudasama B, Patel R, Upadhyay RV, Mehta RV. Field induced rotational viscosity of ferrofluid: effect of capillary size and magnetic field direction. J Colloid Interface Sci 2008; 323: 153–157.
35. Roch A, Gossuin Y, Gillis P, Muller RN. Superparamagnetic colloid suspensions: water magnetic relaxation and clustering. J Magn Magn Mater 2005; 293: 532–539.

